An integrated approach to simulating the vulnerable atherosclerotic plaque

Navid Mohammad Mirzaei,
Department of Mathematical Sciences,
University of Delaware,
DE 19716

William S. Weintraub
MedStar Heart and Vascular Institute,
MedStar Washington Hospital Center
Washington DC 20010

Pak-Wing Fok
Department of Mathematical Sciences,
University of Delaware,
DE 19716
pakwing@udel.edu

Short Title: Simulating atherosclerotic plaque
Word Count: 8874

Abstract

Analyses of individual atherosclerotic plaques are mostly descriptive, relying - for example – on histological classification by spectral analysis of ultrasound waves or staining and observing particular cellular components. Such passive methods have proved useful for characterizing the structure and vulnerability of plaques but have little quantitative predictive power. Our aim is to introduce and discuss a computational framework to provide insight to clinicians and help them visualize internal plaque dynamics.

We use Partial Differential Equations (PDEs) with macrophages, necrotic cells, oxidized lipids, oxygen concentration and PDGF (Platelet Derived Growth Factor) as primary variables coupled to a biomechanical model to describe vessel growth. The model is deterministic, providing mechanical, morphological, and histological characteristics of an atherosclerotic vessel at any desired future time point. We use our model to create computer-generated animations of a plaque evolution that are in qualitative agreement with published serial ultrasound images and hypothesize possible atherogenic mechanisms.

A systems-biology model consisting of 5 differential equations is able to capture the morphology of necrotic cores residing within vulnerable atherosclerotic plaque. In the context of the model, the distribution of Ox-LDL particles, endothelial inflammation, plaque oxygenation (via the presence of vasa vasora) and intimal oxygenation are four important factors that drive changes in core morphology.

New and Noteworthy

In this article, we propose a quantitative framework to describe the evolution of atherosclerotic plaque. We use Partial Differential Equations (PDEs) with macrophages, necrotic cells, oxidized lipids, oxygen concentration and PDGF as primary variables coupled to a biomechanical model to describe vessel growth. A feature of our method is that it outputs color-coded vessel sections corresponding to regions of the plaque that are necrotic and fibrous, qualitatively similar to images generated by enhanced intravascular ultrasound.

1. Introduction

Cardiovascular disease affected more than 121 million people in 2016 in the United States and about 48% of adults (4). It is often due to atherosclerosis, which manifests itself as a buildup of fatty deposits mainly in the intima of medium-sized and large arteries. Plaques exhibit considerable variability in their internal structure and histology. When they develop a thin cap and a large necrotic core, they are prone to mechanical rupture (49), which often results in thrombosis and acute events such as myocardial infarction (MI). The prediction of plaque progression and rupture remains one of the most important open problems in cardiovascular disease today.

Figure 1 shows the main actors involved in atherogenesis. Healthy endothelial cells produce a certain amount of nitric oxide (NO) which is a vasodilator. A decrease in laminar shear stress reduces the production of this chemical which could lead to endothelial dysfunction, increased uptake of low density lipoproteins (LDL) and upregulation of Vascular Cell Adhesion Molecule-1 (VCAM-1). This adhesion molecule starts an inflammatory process by binding with Intracellular Adhesion Molecule-1 (ICAM-1) on the surface of leukocytes present in the blood stream. Attached to the endothelium, monocytes penetrate the vessel wall in response to chemoattractants such as MCP-1 and transform into macrophages in the presence of macrophage colony stimulating factor (M-CSF). LDLs in the intima go through oxidization, turning into oxidized LDLs (Ox-LDL). Macrophages may release more chemoattractant, thereby starting a cascade of inflammation. While they preferentially consume oxidized LDLs and turn into foam cells, Smooth Muscle Cells (SMCs) can also migrate into the plaque from the underlying media and consume Ox-LDLs, albeit at a slower rate. The death of SMCs, foam cells and macrophages all contribute to a necrotic core, one of the defining characteristics of a vulnerable (rupture-prone) plaque (50,32).

Atherosclerosis has been studied from cellular (3), genetic (15) and clinical (6) perspectives. Murine models have also proved valuable in elucidating the main aspects of early-stage atherosclerosis (44). However, one set of tools that remains under-utilized is the application of deterministic mathematical models. Historically, the analysis of plaque has been descriptive or statistical. Scientists may observe an individual plaque at a single time point or gather statistics from large cross-sectional studies. In either case, it is difficult to make predictions from observations at a single time point. In cross-sectional studies, individual risk-factors are assessed using statistical methods, but this approach may not be able to establish causal

relationships. In this article, we advocate a paradigm shift to study the natural history of individual plaques using mathematical models. Combined with advances in imaging technology, we believe that such quantitative approaches will be pivotal in enhancing our understanding of the mechanisms of atherogenesis and plaque rupture. We believe that the best way to characterize the data being generated by imaging modalities such as ultrasound, optical coherence tomography (OCT) and palpography is by connecting them to, and concurrently developing, mathematical models.

In this article we will first review some paradigmatic models of atherosclerotic plaque that are popular in the engineering and mathematical communities. We then show how elements of these models can be combined into a biologically motivated, computer-generated animation that illustrates plaque progression in terms of thickening of arterial layers, deformation of the vessel wall and changes in plaque histology.

2. Methods

Plaque histology. Plaque internal structure has been gradually elucidated since around the 1960s (22). Researchers now believe that the internal structure of a plaque primarily determines its stability. Early plaques start life as "intimal cushions," "intimal thickenings" or "intimal xanthomas" (48). These are relatively innocuous lesions. Over time, however, they can progress into "fatty streaks" which have a higher lipid content. Atheromas have regions of interior necrosis and are considered more dangerous since they are associated with cardiovascular events, e.g. stroke or myocardial infarction.

Enhanced ultrasound (virtual histology) protocols use machine learning to analyze the frequency content in ultrasound waves and classify atherosclerotic tissue into four different types: fibrous, fatty, necrotic and calcific (39). The resulting patterns are fascinating and thought-provoking. For example, Kubo et al (2010) tried to gain insight into the dynamic evolution of plaque histology and morphology (30). Figure 2 shows serial IVUS images of plaque at baseline and after a 12 month follow-up. Data specific to individual plaques at these two time points were also collected. For example, morphological characteristics such as the area occupied by the lumen and fraction of the plaque occupied by the necrotic core were observed. This data set raises several important quantitative questions. How long does it take for a plaque to become vulnerable to rupture? How quickly do plaques grow in size? How quickly do regions of necrosis grow? How does necrosis affect the likelihood of rupture? All these questions can, in principle, be answered by a mathematical model of plaque development, properly calibrated against suitable data sets.

A popular method in the mathematical modeling community is the application of differential equations. This approach describes how concentrations of certain cell types and metabolites change in time. One well-known example is Hao and Friedman's model (24). They described the movement of macrophages, T-cells and

smooth muscle cells into the intima, which promote intimal thickening. Their model however, did not consider the mechanical properties of the intima and neglected the other two layers of the vessel wall. Chalmers et al. used differential equations to explore the dynamics of early atherosclerosis (10). Their model considered the concentration of LDLs, chemoattractants, Endothelium-Stimulating (ES) cytokines, macrophages and foam cells. All of their simulations were done in one dimension and their result provided qualitative and quantitative insight into the effect of LDL in the inflammatory response. In another paper, Chalmers et al. further investigated the effect of High Density Lipoproteins (HDL) in plaque regression (9). They observed that increasing HDL influx regresses plaques with a low density of foam cells and slows the growth of plaques with a high density of foam cells. El Khatib et al. suggested that inflammation propagates in the intima as a reaction diffusion wave (18). They concluded that in the case of intermediate LDL concentrations there are two stable equilibria: one corresponding to the disease-free state and another for the inflammatory state, while a traveling wave connects these two states. Fok investigated the effect of the spatial distribution of Ox-LDL on the location and size of the necrotic core (19). He predicted the location and size of the necrotic core due to the chemotaxis of macrophages towards sources of Ox-LDLs and their death due to lack of oxygen. Finally, Cobbold et al. investigated the multiple stages of LDL oxidation using a system of ordinary differential equations (14). In their model, they considered the concentration of antioxidants (specifically vitamin E and vitamin C), HDL, LDL and free radicals. They modeled how HDL and vitamin C were crucial for for slowing down the oxidation of LDL particles.

Cardiovascular research is not limited to processes occurring in the arterial wall. Blood flow also plays an important role in atherogenesis. Changes in the laminar shear stress or the concentration of different chemicals within the bloodstream are some of the crucial factors that can affect the composition of arteries. Therefore, investigating the early stages of atherosclerosis as a fluid-solid interaction (FSI) problem has attracted many researchers (12, 16, 8). As well as coronary arteries, there are studies that utilize FSI in other types of arteries. For example, Pozzi and Vergara investigate the carotids (40) while Thon et al. study aortic arteries (46). Their approaches can be adapted for coronary arteries with minor modifications.

In this paper we consider a simple system of Partial Differential Equations (PDEs) that could describe the formation of hypoxia-induced plaque cores:

$$\underbrace{\frac{\partial N}{\partial t}}_{\substack{\text{Rate of increase}\\ \text{of NCs}}} = \underbrace{D_1 \Delta N}_{\substack{\text{Diffusion of}\\ \text{NCs}}} + \underbrace{\gamma(C)M}_{\substack{\text{Generation of NCs}\\ \text{from dead}\\ \text{macrophages}}} - \underbrace{\beta_1 N}_{\substack{\text{Clearance of NCs by}\\ \text{other leukocytes}}} \quad (1)$$

$$\underbrace{\frac{\partial M}{\partial t}}_{\substack{\text{Rate of increase}\\ \text{of MCs}}} + \underbrace{\nabla.\left(\mu M \nabla (L+Q)\right)}_{\substack{\text{Chemotaxis to Ox-LDL}\\ \text{and CKs}}} = \underbrace{D_2 \Delta M}_{\substack{\text{Diffusion}\\ \text{of MCs}}} - \underbrace{\gamma(C)M}_{\text{Hypoxic Death}} \quad (2)$$

$$\underbrace{\frac{\partial Q}{\partial t}}_{\substack{\text{Rate of increase}\\ \text{of CKs}}} = \underbrace{D_3 \Delta Q}_{\substack{\text{Diffusion of}\\ \text{CKs}}} - \underbrace{\beta_2 Q}_{\substack{\text{Natural decay}\\ \text{of CKs}}} + \underbrace{\lambda_1 LM}_{\substack{\text{Production}\\ \text{of CKs}}} \quad (3)$$

$$\underbrace{\frac{\partial C}{\partial t}}_{\substack{\text{Rate of increase}\\ \text{of oxygen}}} = \underbrace{D_4 \Delta C}_{\substack{\text{Diffusion of}\\ \text{oxygen}}} - \underbrace{\beta_3 C}_{\substack{\text{Background}\\ \text{consumption}\\ \text{of oxygen}}} - \underbrace{\lambda_2 CM}_{\substack{\text{Consumption of oxygen}\\ \text{by macrophages}}} + \underbrace{f(x,y,t)}_{\substack{\text{Oxygen}\\ \text{sources}}} \quad (4)$$

$$\underbrace{\frac{\partial P}{\partial t}}_{\substack{\text{Rate of increase}\\ \text{of PDGF}}} = \underbrace{D_5 \Delta P}_{\substack{\text{Diffusion of}\\ \text{PDGF}}} - \underbrace{\beta_4 P}_{\substack{\text{Natural decay}\\ \text{of PDGF}}} \quad (5)$$

These equations are supplemented with boundary conditions (BCs):

$$\frac{\partial N}{\partial \boldsymbol{n}_1} = 0 \quad \text{on } \partial\omega_1 \qquad (6) \qquad\qquad \frac{\partial N}{\partial \boldsymbol{n}_2} = 0 \quad \text{on } \partial\omega_2 \qquad (7)$$

$$M = M_0(t) \quad \text{on } \partial\omega_1 \qquad (8) \qquad\qquad \frac{\partial M}{\partial \boldsymbol{n}_2} = \kappa M \quad \text{on } \partial\omega_2 \qquad (9)$$

$$\frac{\partial Q}{\partial \boldsymbol{n}_1} = 0 \quad \text{on } \partial\omega_1 \qquad (10) \qquad\qquad \frac{\partial Q}{\partial \boldsymbol{n}_2} = 0 \quad \text{on } \partial\omega_2 \qquad (11)$$

$$C = C_0(t) \quad \text{on } \partial\omega_1 \qquad (12) \qquad\qquad \frac{\partial C}{\partial \boldsymbol{n}_2} = 0 \quad \text{on } \partial\omega_2 \qquad (13)$$

$$P = P_0 \quad \text{on } \Gamma \subset \partial\omega_1, \quad P = 0 \quad \text{on } \partial\omega_1 \setminus \Gamma, \qquad (14)$$

$$\frac{\partial P}{\partial \boldsymbol{n}_2} = 0 \quad \text{on } \partial\omega_2 \quad (15)$$

The boundaries $\partial\omega_1$, $\partial\omega_2$ and Γ and the vectors $\boldsymbol{n}_1$and $\boldsymbol{n}_2$ are indicated in Figure 3. Variables N, M, Q, C and P represent concentrations of necrotic cells (NCs), macrophage cells (MCs), a chemokine (CK) such as Monocyte Chemoattracting Protein 1 (MCP1), molecular oxygen and Platelet Derived Growth Factor (PDGF); $D_1 - D_5$ are their diffusivities; μ is a chemotactic coefficient for macrophages; $\beta_1 - \beta_4$ are decay coefficients; λ_1 is a production rate of MCP1; λ_2 is the consumption rate of oxygen by macrophages and κ is the outflux rate of macrophages from the intima to media (see Table 1 for a summary). Furthermore, we take the concentration of Ox-LDL (L) to be a known function in space and time. In our problem, most of the

histological dynamics occur much more quickly than the growth of the plaque. Therefore, equations (1)-(5) are all solved at steady state. On the other hand, we assume that the time scales associated with endothelial inflammation, arterial oxygenation and changes in Ox-LDL density are on par with that of the plaque growth and the time dependence of $M_0(t)$, $C_0(t)$ and $f(x, y, t)$ is explicitly accounted for.

In eq. (1), the term on the left hand side represents the time rate of change of necrotic cells at a given point **x** = *(x,y,z)* in the plaque. This equation specifies that the rate of change of NCs at **x** has three contributions. First, NCs from nearby points **x**+δ**x** can be moved to **x**. This diffusion could arise from immune cells in the plaque exerting random forces on dead cells through their own random motion. Second, macrophage cells at **x** can die and become necrotic, essentially converting from vital cells to necrotic ones. The death rate γ depends on the oxygen concentration at that point, *C(x,y,z)* via the equation (19)

$$\gamma(C) = \gamma_{\min} + (\gamma_{\max} - \gamma_{\min})\left(\frac{C_{\text{crit}}^m}{C_{\text{crit}}^m + C^m}\right). \quad (16)$$

The normoxic death rate $\gamma_{\min}$ is the death rate for macrophages in an oxygen-sufficient environment and $\gamma_{\max}$ is the hypoxic death rate in an oxygen-limited environment. The last term in parentheses is called a Hill function and the number m is called the Hill coefficient (we take m=4). Eq. (16) states that macrophages die quickly when oxygen levels are low ($C<C_{crit}$), but slowly when levels are high ($C>C_{crit}$). We see that C_{crit} acts as a hypoxic threshold for macrophage cells and the larger the value of m, the more abrupt the switch. Finally, NCs at **x** can be cleared by leukocytes and the clearance rate is proportional to the number of NCs. The minus sign signifies that the clearance term *reduces* the rate of generation of NCs.

In eq. (2), the first term on the left hand side represents the time rate of change of MCs. The second term represents chemotaxis, the directed movement of cells towards chemoattractants such as Ox-LDL (L) and MCP1 (Q). Macrophages chemotax along the vector $\nabla(L + Q)$ with associated "flux" $\mu M \nabla(L + Q)$ and the coefficient μ capturing the speed of taxis. Note that $\nabla(L + Q)$ is a vector that points from small values of L+Q to large values so MCs are modeled to move from low to high concentrations of total chemoattractant. There are two contributions on the right hand side. Similar to eq. (1), the first term represents the diffusion of the cells. The final term represents the death of macrophages with a death rate dependent on the local oxygen concentration C as given by eq. (16). The $+\gamma(C)M$ in eq. (1) and $-\gamma(C)M$ in eq. (2) couple the equations together: when a macrophage cell dies, it converts to a necrotic cell.

In eq. (3), the term on the left hand side represents the time rate of change of CKs. Similarly, we have three terms on the right hand side. The first term corresponds to the diffusion of the CKs. The next term represents the natural decay of CKs at a rate β_2. The last term represents the production of CKs by MCs after consumption of Ox-

LDL at a rate λ_1. Motivated by the principle of mass action, the production rate is proportional to the product of macrophage and Ox-LDL concentrations, *LM*. The net production is greater if there are more MCs or Ox-LDL particles.

In eq. (4), the term on the left represents the time rate of change of the oxygen concentration. The first term on the right hand side corresponds to the diffusion of oxygen in tissue. The second term represents the background consumption of oxygen by all cells (excluding MCs) with rate β_3. The third term represents the consumption of the oxygen concentration by macrophages at a rate λ_2. Again, motivated by mass action principles, the net consumption rate is proportional to the product of oxygen concentration and macrophage density, *CM*. The final term represents contributions from oxygen sources such as microvessels that could be present in advanced plaques.

In eq. (5), the term on the left represents the time rate of change of the PDGF concentration. The first term on the right represents the diffusive spread of PDGF. The second term corresponds to the natural (thermal) degradation of PDGF at a rate β_4.

Boundary conditions (8), (12) and (14) prescribe the concentration of macrophages, oxygen and PDGF at the endothelium while BCs (6) and (10) account for the *flux* of necrotic cells and MCP1 across the endothelium $\partial\omega_1$. Eqs. (7), (9), (11), (13) and (15) prescribe the flux of necrotic cells, macrophages, MCP1, oxygen and PDGF from the intima into the media through the boundary $\partial\omega_2$.

So far, we have explained the physical and biological origins of each of the terms in equations (1)-(5). The validity of these equations relies on the continuum assumption: rather than describing the behavior of individual cells, we are calculating their aggregate or average behavior using smooth functions. While this can be a limitation, there are more advanced methods that can be used to capture individual cell behavior (17). Furthermore, the transport properties of the vessel wall have to be homogeneous for the equations to hold. At a molecular level, the random motion of cells and chemicals must follow a Brownian motion which results in diffusive PDEs. Finally, we have only focused on a small set of cell-cell, cell-cytokine and cell-substrate interactions, ignoring for example M-CSF induced monocyte-macrophage transformations and durotactic effects.

In principle, the solution of equations (1)-(5) produces *N*, *M*, *Q*, *C* and *P* as smooth functions of space and time, representing densities of NCs, MCs, CKs, O_2 and PDGF. When the governing equations are solved in practice, these quantities all find their equilibrium levels very quickly compared to the observed rate of plaque progression so the steady-state, time *independent* versions of (1)-(5) are actually computed by setting all time derivatives to zero. An example of the function *N* is shown in Figure 4, along with a thresholding method to formally distinguish between necrotic and fibrous tissue. To solve the equations, one needs the values of

all the constants $D_1 - D_5$; $\beta_1 - \beta_4$; μ, λ_1, λ_2 , $\gamma_{\min}, \gamma_{\max}, C_{\text{crit}}$ and the Hill coefficient *m.* These constants can be found from experiments or estimated independently.

Plaque Morphology and Mechanics. In addition to describing the plaque's histology through PDEs, it is also important to describe the stresses within a plaque. Virmani et al. (49) have shown that plaques are more likely to rupture if their caps are thin (<65 um). This observation becomes intuitive after we understand that caps in fibroatheromas rupture when they are stressed beyond a threshold yield stress (33). As cap morphology evolves over time, so do the associated stress fields and the propensity for rupture. Therefore an integrated model of vulnerable plaque should also explain how stress and strain fields evolve and couple these fields to tissue growth and atrophy.

Mechanics and Deformation. Leonhard Euler (1707-1783) was possibly the first person to use mathematics to formulate models for arterial mechanics. His calculations described how the pulsatility of blood flow affected the expansion of arterial cross sections. By the 1970s arterial hemodynamics was a mature field and in the 1990s the mechanical properties of tissues became a core focus. Aided by developments in numerical methods for fluid mechanics and solid-fluid interactions, simulation of the cardiovascular system became a highly evolved enterprise (45, 21, 41). The ubiquity and power of computers allowed researchers to predict the deformations of the arterial wall and the hemodynamics contained within to an unprecedented level of detail. For example, Simon et al. developed a computational method based on the poroelasticity of arterial tissues (43). Their model coupled the wall deformation, fluid mechanics and associated transport phenomena in the arterial wall. Auricchio et al. investigated the biomechanical reaction of a stenotic artery wall to an expandable stent (2). Their aim was to understand the mechanisms underlying stent-related restenosis. Finally, Akyildiz et al. studied the effect of intima stiffness and plaque morphology on maximum plaque stress (1). They found that reducing cap thickness and increasing the size of the necrotic core increased the peak stress.

The finite element method is a very versatile method which can be used for solving both dynamic and static problems. Most of the approaches outlined above utilize this method for computing the equilibrium configuration of an elastic artery under a given load. This framework can be adapted to accommodate a model of tissue growth called morphoelasticity. The underlying assumption is that growth occurs so slowly that mechanical equilibrium is maintained at all times. Below, we describe the elastostatics problem, and then explain how morphoelasticity can be used to evolve the plaque dynamically.

Elastostatics. The deformation vector tracks the position of every material point in the artery under a given load and maps a *reference configuration* to a *deformed configuration*. The starting point for our method is an energy integral that accounts for all the ways that deformations affect the total energy. This usually consists of three parts. First, there is the stored potential energy associated with deformations

from an unstressed, reference state. Second, there is the energy associated with the deformations doing work against body forces (such as gravity). Finally the deformations also do work against surface forces (such as a lumen pressure). While deformations of the elastic body increase the energy, any work done against body and surface forces require energy and is subtracted from the total budget. In the absence of growth we have:

$$\Pi[\Phi] = \int_{\Omega} W(\nabla\Phi)\, dV - \int_{\Omega} f(\Phi)\, dV - \int_{\partial\Omega} g(\Phi, \nabla\Phi) dS, \qquad (17)$$

where Π is the total energy, Φ is the deformation vector, f and g are body and surface force densities, Ω is the "reference domain" (points in space occupied by the unloaded artery), and $\partial\Omega$ is the mathematical boundary between the lumen and the undeformed vessel wall. The strain energy density of the elastic artery is W and depends on the deformation *gradient* $\nabla\Phi$. A quick way to understand this is that the energy should depend on the change in the dimensions of an infinitesimal cuboid relative to its dimensions in the reference configuration. In other words, the energy does not depend on the deformation vector Φ but rather on how Φ changes when applied to neighboring points in the reference configuration. To find the arterial deformation, one first defines the mechanical properties of the vessel wall by specifying W. For example, it may be mechanically anisotropic (collagen fibers in the vessel make it harder to stretch radially, than axially); or it may be layer-dependent (mechanical properties of the intima are different than the media or adventitia). We employ a layer-specific strain energy following (27) which comes from *ex-vivo* stress tests of arterial tissue. For more details on the strain energy see (36).

For most arterial problems, body forces such as gravity are negligible so $f = 0$. For a lumen pressure p, one can show that the surface force density is in fact

$$g(\Phi, \nabla\Phi) = -\frac{p}{3} J(\nabla\Phi)^{-T} N \cdot \Phi \qquad (18)$$

where $J = \det \nabla\Phi$ and N is the unit outward normal vector to $\partial\Omega$. The ultimate objective is to find the deformation Φ that minimizes Π in (17). This high-dimensional optimization problem is solved computationally. Once Φ is known, the displacement of every point in the reference configuration determines the deformed configuration: see Figure 5 for how the finite element mesh deforms under the effect of Φ. More details can be found in textbooks such as (26). In this paper we take p to be the average of systolic and diastolic blood pressure. Since atherosclerosis is always associated with high blood pressure we take $p=120$ mmHg, which according to the American Heart Association corresponds to stage II hypertension.

Tissue Growth and Morphoelasticity. The way we account for tissue growth in our model is by employing the theory of morphoelasticity (23, 51). Eq. (17) above depends on the deformation gradient $\mathbf{F} = \nabla\Phi$ which captures how an infinitesimal cuboid of tissue changes dimensions under a deformation Φ. Since biological tissue

mostly consists of water, the volume of the cuboid is approximately conserved as it is strained. The consequence is that the total volume of the reference and deformed arteries are almost identical. However, in morphoelasticity we assume that tissue first undergoes a stress-free volumetric growth (characterized by a growth tensor) before being strained. Specifically, an element first responds to a pure growth meaning that it increases its volume by a specified amount. This will cause an "overlap" with neighboring elements resulting in an incompatible configuration. Therefore by itself, the growth tensor does not give a physical configuration and needs to be followed by a corrective strain, characterized by an elastic tensor. The resulting compound process guarantees that the outcome is a continuous grown domain with no overlaps. Mathematically the process assumes that the deformation gradient can be written as a product of the growth tensor ($\mathbf{F_g}$) and the elastic tensor ($\mathbf{F_e}$):

$$\mathbf{F} = \mathbf{F_e}\mathbf{F_g}, \qquad (19)$$

see Figure 6. The energy in (17) also needs to be modified under this assumption of growth: for details, see (20).

How does morphoelasticity help with plaque modeling? The growth tensor $\mathbf{F_g}$ can be informed by the biology of atherosclerosis. From murine models the initial stages of plaque growth are characterized by an increase in intima mass, resulting from a migration of smooth muscle cells from the media (13). One possible trigger for this migration is PDGF (29). In our model, we simplify this process by assuming that PDGF is directly responsible for growth and take $\mathbf{F}_g = \begin{pmatrix} g_1 & 0 & 0 \\ 0 & g_2 & 0 \\ 0 & 0 & 1 \end{pmatrix}$: increments of arterial tissue increase their radial and circumferential dimensions by g_1 and g_2 respectively and we let g_1 and g_2 depend on PDGF concentration (as predicted by equation (5)) through a Hill function so that

$$g_k = \exp\left(\alpha_k \int_0^t \frac{P^m}{P^m + P_0^m}\, dt'\right), \qquad (20)$$

where $\alpha_1 = 1$, $\alpha_2 = 0.25$, $m = 4$ and $P_0 = 1.12*10^{-5}$ mol/L (these constants were chosen for convenience). The growth tensor is a crucial element of the model because it allows the histological and morphoelastic models to communicate with each other. However, one has to be careful about constructing the growth tensor from the PDGF distribution. The growth tensor is always applied to the reference domain: recall eq. (19). However, the PDGF equation (5) - like the other PDEs - is solved in the deformed domain. Because there is a one-to-one correspondence between mesh elements in the reference and deformed configurations (see Fig. 5), the PDGF concentration in a reference element is simply taken as the value that was computed for the corresponding deformed element. Using this method, we define a

spatially varying PDGF distribution in the reference domain that can be used to update eq. (20) at each time step.

The resulting *integrated* model of atherosclerosis allows us to understand how morphological features of plaque (e.g. lumen size, stenosis, necrotic fraction) could be affected by microbiology (e.g. Ox-LDL density, glucose concentrations, PDGF density) and can be summarized by the following processes:

- Oxidized LDLs infiltrate the intima and diffuse.
- Macrophages chemotax towards oxidized LDLs, consume them and release MCP1, attracting more macrophages.
- Macrophages die if oxygen levels are low, producing necrotic cells.
- PDGF released from platelets induces growth of neo-intima.

Together, these four processes are able to produce a vast range of morphological and histological changes in the vessel. Our simulations are done in two dimensions since plaque structure is often presented in two-dimensional arterial cross sections. Our computations are carried out in the FEniCS finite element computational environment using the University of Delaware's Caviness cluster. The coupling of PDEs (1)-(4) is done by introducing a "mixed" finite element space (31), consisting of the Cartesian product of individual (first order) finite element spaces. Specifically, Newton's iteration finds a vector (N,M,Q,C) that makes the weak form of (1)-(4) and (6)-(13) stationary for all test functions drawn from the mixed space: see Figure 7 for a flowchart of the algorithm. The time step used for our simulations is $\Delta t = 0.004$ months. With this value of Δt, the growth functions $g_k(t)$ (eq. (20)) are approximated using Simpson's integration rule at $t = t_j = j\Delta t, j = 0, 1, 2, \ldots$ and the time-dependent functions $C_0(t)$, $M_0(t)$, $f(x,y,t)$ and $L(x,y,t)$ in eqs. (8), (12), (4) and (2,3) are directly evaluated at $t = t_j$. One possible realization of the model at a single time point is shown in Figure 8. We see that oxygen and macrophages are localized near the arterial lumen; a single localized injury to the endothelium has released PDGF, leading to elevated levels of the growth factor near the lower part of the lumen; and a large necrotic core has resulted from the death of many MCs deep in the intima.

3. Results.

Now we illustrate the results of our model. Although there are many ways to produce different plaque outcomes, we focus on changing 4 parameters over time, reflecting 4 main mechanisms that are thought to be associated with inflamed plaques:

1- *Changes in Ox-LDL distribution, $L(x,y,t)$.* It has long been hypothesized that modified LDLs are atherogenic since they are mainly responsible for the appearance of the foam cell phenotype (7). The Ox-LDL density inside a

plaque is governed by the function L whose time evolution we control directly in the model.

2- *Changes in inflammation,* $M_0(t)$ *.* We define inflammation in the endothelium as the density of macrophages adsorbed on the layer. Mathematically we control this density through the boundary condition (8). Biologically, an increasing $M_0(t)$ corresponds to an endothelium that becomes more inflamed over time.

3- *Development of vasa vasora, f(x,y,t)*. Vasa vasora are a network of small vessels that supply the arterial walls with resources such as oxygen and glucose. Sources of oxygen are controlled in our model through the function *f(x,y,t)* in equation (4).

4- *Increase in oxygenation,* $C_0(t)$*.* Arterial oxygenation can depend on intercirculatory mixing, hemoglobin concentration and other systemic factors (34). For example, exercise can increase hemoglobin levels and blood flow to tissues (5) and has also been shown to increase arterial oxygenation in patients with chronic heart failure (25, 42). We control $C_0(t)$ using the Dirichlet boundary condition (12).

A summary of these functions is provided in Table 2. In addition to these four mechanisms, intimal growth depends on PDGF (*P)* through eq. (20). Mathematically, we impose $P = P_0$ for $\boldsymbol{x} \in \partial\omega_1$ with $P_0 > 0$ on n = 0, 1 or 2 small segments of $\partial\omega_1$, representing discrete injury points on the endothelium, and $P_0 = 0$ otherwise. The number of injury points n is fixed in each case and how quickly the plaque grows can be controlled through n.

Now we make connections to the enhanced IVUS images from Kubo's paper (30). In this study, the authors imaged the same plaques 12 months apart to gain insight into their natural history (see Figure 2). There are 5 cases: A-E. To recreate these evolutions, the following protocols were used. Our parameters are separated into two types: those that can potentially change in time and reflect the 4 mechanisms described above, and those that remain static in time (but can differ from case to case). The quantities L, M_0, C_0 and f are in the first category (see Table 2) and all other parameters are in the second (see Table 1). The virtual plaques are evolved over a period of 12 months (up to t = 3 in simulation time) and tissue was defined as necrotic when N exceeded a threshold of 1.4×10^6 cells/cm^3; otherwise the tissue was classified as fibrotic (see Figure 4). Other components (calcific, lipidic) were not directly accounted for by the model. Our simulation results are shown in Figure 9, which should be compared to Figure 2. Parameter values for each of cases A-E are given in Tables 1 and 2. Computer-generated animations of all five plaque evolutions can be found in the Figshare repository (37); see

https://doi.org/10.6084/m9.figshare.11968722.v3.

Case A results from a combination of mechanisms 2 and 4. Endothelial inflammation increases slightly and macrophages chemotax towards sources of Ox-LDL and chemokine. Regions of the intima close to the lumen are more oxygenated and more oxygen in the intima reduces macrophage death from hypoxia. The result is plaque growth along with a necrotic core that "drifts" deeper into the plaque, in rough qualitative agreement with the IVUS results in Figure 2A.

Case B is achieved through mechanisms 1 and 2. For our simulations we assumed that endothelial injury is quickly healed (so there are no sources of PDGF) and that both the Ox-LDL concentration in the intima and macrophage density at the endothelium reduce over time. These effects lead to a vanishing necrotic core.

Case C results from mechanism 1. By changing the location of Ox-LDLs, we were able to alter the direction of macrophage chemotaxis. Because NCs are continuously produced by MC death, the necrotic core follows the macrophage density and moves to the right when the Ox-LDLs move to the right.

Case D results from a combination of mechanisms 1 and 2. The Ox-LDL concentration follows a combination of Gaussian functions with peak densities that increase in time (36). The location of Gaussians was chosen in order to produce the crescent-shaped necrotic core in Figure 2(D). Endothelial inflammation also increases in time. There are low levels of oxygen throughout the intima and PDGF concentrations are maximal at 1 and 7 o'clock. The NC appears in a crescent shape adjacent to the lumen from 3 to 5 o'clock.

Finally, Case E results from mechanism 4. Changes in the *spatial distribution* of microvessels are key to producing the pair of images in Case E of Figure 2 (36). There are several regions of necrosis in the baseline state but they are dynamic and increase in number and size in the follow-up case. The seemingly random spatial distribution of necrosis in the follow-up could result from changes in the number and density of vasa vasora in the intima, reflected by taking f to be a function that changes both temporally and spatially.

For more details on dynamics of other concentrations such as macrophages, Ox-LDLs, MCP-1, oxygen and PDGF for cases A-E see (36).

4. Discussion

Plaques present considerable inter-patient variability, depending on location and age of the plaque, local and global cell biology, personal genetics, and environmental and lifestyle factors. It is not surprising that the associated evolutions seem hopelessly complicated. We advocate that integrated mathematical models may help with understanding how plaque complexity results from microbiology.

In this paper we assumed that equations (1)-(17) are universal, applying to all plaques (this assumption will be further discussed below) and different plaque

states and evolutions are characterized by different parameters. Studying plaques through these equations is still daunting because there are 21 different parameters and functions in Tables 1 and 2. While we estimated them for the purposes of matching the IVUS images in Figure 2, in principle each one should be measured *in-vivo* for a particular patient. Although this may not be practical or even possible, there are two reasons why the model could still be valuable. First, even though the parameters and driving functions are unknown, they could be estimated from *in-vitro* experiments or from animal models. Knowledge of more parameters gives the model more predictive power and puts the study of plaque on a more rigorous scientific footing. Second – and more importantly – the integrated model can be systematically tested and recalibrated to accommodate new data. Rather than passively describing plaques and accumulating observations, the integrated model puts clinicians in the driving seat, enabling them to formulate and test new hypotheses.

There is the remaining issue that equations (1)-(17) are probably *not* universal. However, this does not pose any added conceptual difficulty providing experimentalists, clinicians and theorists closely collaborate. Instead of updating parameter values, individual terms in the equations can be modified to reflect the latest data. New equations can even be included (or removed) if required. The power of a mathematical model is that it can be continuously refined and updated in light of new scientific developments.

Caveats and Limitations

The model presented in this paper focused on six main quantities: necrotic cells, macrophage cells, Monocyte Chemotactic Protein, Platelet-Derived Growth Factor, oxygen and oxidized LDLs. This is a minimal model: for example we have not distinguished between M1 and M2 macrophages (M1s are thought to be pro-inflammatory while M2s are atheroprotective); neither have we accounted for hemodynamics, the effect of glucose, or the intricate biology of cell death. However, the extension to these more complex cases is not conceptually more difficult in terms of PDE modeling. In principle one can write down as many equations as the biology demands. Physical laws realized through a mathematical framework provide systematic ways to do this that are consistent with principles of mass conservation and continuum mechanics. The main technical hurdle is not in the mathematical modeling but in finding parameter values and making comparisons with data. To do this requires careful calibration of the model output with serial images such as Figure 2. It also requires close collaboration between mathematicians/engineers and clinicians/imaging specialists.

Our model was mostly focused on a structural model of plaque that can be affected by local intimal growth. Therefore, we focused on a 2D domain, following IVUS images. We are aware that an arterial model is not complete without blood flow dynamics. In reality, endothelial permeability is impacted by laminar wall shear stress which changes Ox-LDL deposition rates and triggers the intimal inflammatory cascade: all other atherosclerotic biomechanical and chemical responses follow,

including platelet production of PDGF. However, in this paper the locations of endothelial dysfunction, (Γ in Fig. 3) as well as the Ox-LDL distribution were imposed without considering any hemodynamics. If we considered a 3D arterial geometry and included hemodynamics into our model, the tissue mechanics simulation would be more computationally intensive and Γ would be a 2D surface rather than a curve segment, and determined as a result of blood flow rather than decided *a priori*. Solution of the blood flow equations in a 3D lumen and coupling them to the tissue mechanics would certainly increase the complexity of the model.

When lumen pressure is removed from arterial segments *ex-vivo*, a stress called a residual stress still remains: this can be seen when a radial cut is made, usually causing the segment to spring open. Another limitation of the current model is that we have not accounted for residual stresses (11) in the arterial segments at baseline. The residual stress can alter the total Cauchy stress after pressurization and growth, so predictions of stress must be made very carefully with this model. Incorporating the effects of residual stress can be done by modifying the reference configuration (47).

Other chemical messengers can be incorporated into the model depending on what is suggested by imaging data. Currently, enhanced IVUS provides spatially resolved maps of necrosis, cholesterol and calcium phosphate *in-vivo*. While other cytokines such as interleukins (35, 28) also play an important role in the development of plaques, including them into our model does not provide additional insight if there are no data to indicate their spatial distribution and temporal evolution; in fact including their effect would only increase the number of unknown parameters in our model and therefore the uncertainty of the predictions. Histological stains such as Movat and Haematoxylin & Eosin (H&E) constitute the "gold standard" in terms of determining spatial data within the plaque. If these stains can be used in an animal study in which animals are periodically sacrificed and particular arteries analyzed in terms of cell positions and cell types, this experimental protocol could provide more information about the dynamics within a plaque and further inform our integrated model.

Future Challenges

We believe that the future for quantitative models of atherosclerosis is promising. Imaging technologies such as OCT and infrared spectroscopy are giving us the ability to visualize the evolution of plaque morphology and composition. The great challenge at the moment is the way the data are being collected. Scientific prediction is concerned with quantifying future states from past states. The more informed we are of past states, the better our prediction of future states. The few existing "natural history" studies of human atherosclerosis have an extremely low time resolution. For example, the plaques in (30) are scanned at just two time instances (a baseline and a follow-up) within a year from each other. Serial studies in single patients need to be performed more frequently, and at greater time resolution. The hurdle here is clinical indication for the procedure. Nevertheless, we believe that high time-

resolution serial studies hold the key to a better understanding of atherosclerosis. Providing modelers and quantitative scientists with more snapshots, or even a movie of disease progression will greatly enhance the modeling and possibly prediction of atherosclerotic development.

Another advance that will greatly help in aiding prediction is an improvement in virtual histology technology and integration with other imaging methods. Currently the master algorithm classifies tissues into four categories: fibrous, fatty, necrotic and calcific. In reality, a given region can share characteristics from each category. For example, necrotic cells could be interspersed with flecks of calcium. What is really needed is a continuous version of the 4 categories. What could such a scale look like? One possibility is to use a vector that represents weights of each category: $p = (p_1, p_2, p_3, p_4)$ where $\sum_{i=1}^{4} p_i = 1$. For example, (0,0,0,1) corresponds to a region that is completely calcified and (0,0,1,0) corresponds to a region that is completely necrotic. However, an area where calcium and necrosis are present in equal amounts can be represented as (0, 0, 0.5, 0.5). Constructing the algorithms to provide this level of detail will prove challenging, since even the current 4-color method is not universally accepted and does not always match the histological gold-standard.

Overall, the mathematical community is well-positioned to make inroads to understanding the patterns seen in enhanced IVUS images or other imaging modalities of atherosclerotic plaque. While the underlying biology in plaque development is intricate and complex, we believe that mathematics provides the conceptual bridge that connects plaque environment to the spatial patterns that ultimately result.

5. Funding

PWF was supported by a Simons Foundation collaboration grant 282579. NMM and PWF were supported by a DE-CTR ShoRe pilot grant NIGMS IdeA U54- GM104941.

6. Acknowledgements

This manuscript has been released as a pre-print at the Arxiv (Mohammad Mirzaei et al. (2019)) (38)

7. Conflict of Interest

None of the authors have any conflicts of interest.

8. Author Contributions

PWF and WSW contributed to the conception and design of the study; NMM performed the simulations; PWF wrote the first draft of the manuscript; NMM and PWF wrote sections of the manuscript. All authors contributed to manuscript revision, read and approved the submitted version.

References

1. Akyildiz, A. C., et al. "Effects of intima stiffness and plaque morphology on peak cap stress." *Biomedical engineering online* 10, no. 1 (2011): 25.
2. Auricchio, F., M. Di Loreto, and E., Sacco. "Finite-element analysis of a stenotic artery revascularization through a stent insertion." *Computer Methods in Biomechanics and Biomedical Engineering* 4, no. 3 (2001): 249 - 263.
3. Bendeck, MP, N Zempo, AW Clowes, RE Galardy, and MA. Reidy. "Smooth muscle cell migration and matrix metalloproteinase expression after arterial injury in the rat." *Circulation research* 75, no. 3 (1994): 539-545.
4. Benjamin, EJ, P Muntner, and MS. Bittencourt. "Heart Disease and Stroke Statistics—2019 Update: A Report From the American Heart Association." *Circulation* 139, no. 10 (2019): e56 - e528.
5. Boone, Tommy. *Introduction to exercise physiology.* Jones & Bartlett Publishers, 2014.
6. Bourantas, Christos V., et al. "Clinical and angiographic characteristics of patients likely to have vulnerable plaques: analysis from the PROSPECT study." *JACC: Cardiovascular Imaging* 6, no. 12 (2013): 1263-1272.
7. Brown, M.S., and J.L., Goldstein. "Lipoprotein metabolism in the macrophage: implications for cholesterol deposition in atherosclerosis." *Annual review of biochemistry* 52, no. 1 (1983): 223 - 261.
8. Calvez, Vincent, Jean Gabriel Houot, Nicolas Meunier, Annie Raoult, and Gabriela Rusnakova. "Mathematical and numerical modeling of early atherosclerotic lesions." *ESAIM: Proceedings* 30 (2010): 1--14.
9. Chalmers, Alexander D, Anna Cohen, Christina A Bursill, and Mary R Myerscough. "Bifurcation and dynamics in a mathematical model of early atherosclerosis." *Journal of Mathematical Biology* 71 (2015): 1451--1480.
10. Chalmers, Alexander D, Christina A Bursill, and Mary R Myerscough. "Nonlinear dynamics of early atherosclerotic plaque formation may determine the efficacy of high density lipoproteins HDL in plaque regression." *PLoS ONE* 12 (2017).
11. Chuong, C. J., and Y. C. Fung. "Residual Stress in Arteries." In *Frontiers in Biomechanics*, by Schmid-Schönbein G.W., Woo S.LY. and Zweifach B.W., 117 - 129. New York: Springer, 1986.
12. Cilla, Myriam, Estefania Pena, and Miguel A Martinez. "Mathematical modelling of atheroma plaque formation and development in coronary arteries." *Journal of The Royal Society Interface* 11 (2014).
13. Clowes, Alexander W., M. A. Reidy, and M. M. Clowes. "Kinetics of cellular proliferation after arterial injury. I. Smooth muscle growth in the absence of endothelium." *Laboratory investigation; a journal of technical methods and pathology* 49, no. 3 (1983): 327-333.
14. Cobbold, CA, JA Sherratt, and SRJ Maxwell. "Lipoprotein oxidation and its significance for atherosclerosis: a mathematical approach." *Bulletin of Mathematical Biology* 64 (2002): 65--95.

15. Cyrus, Tillmann, et al. "Disruption of the 12/15-lipoxygenase gene diminishes atherosclerosis in apo E–deficient mice." *The Journal of clinical investigation* 103, no. 11 (1999): 1597-1604.
16. Di Tomaso, Giulia, Vanessa Diaz-Zuccarini, and Cesar Pichardo-Almarza. "A multiscale model of atherosclerotic plaque formation at its early stage." *IEEE transactions on biomedical engineering* 58 (2011): 3460--3463.
17. DiMilla, PA, K Barbee, and DA Lauffenburger. "Mathematical model for the effects of adhesion and mechanics on cell migration speed." *Biophysical Journal* 60, no. 1 (1991): 15-37.
18. El Khatib, N, S Genieys, and V Volpert. "Atherosclerosis initiation modeled as an inflammatory process." *Mathematical Modelling of Natural Phenomena* 2 (2007): 126--141.
19. Fok, Pak-Wing. "Growth of Necrotic Cores in Atherosclerotic Plaque." *Mathematical Medicine and Biology* 29, no. 4 (2012): 301-327.
20. Fok, Pak-Wing, and Kun Gou. "Finite Element Simulation of Intimal Thickening in Multi-Layered Arterial Cross Sections by Morphoelasticity." *Computer Methods in Applied Mechanics and Engineering* 363, no. 112860 (2020).
21. Franzone, Piero Colli, Luca Franco Pavarino, and Simone Scacchi. *Mathematical cardiac electrophysiology.* Springer, 2014.
22. Geer, Jack C., Henry C. McGill, and Jack P. Strong. "The Fine Structure of Human Atherosclerotic Lesions." *The American Journal of Pathology* 38, no. 3 (1961): 263-287.
23. Goriely, Alain. *The mathematics and mechanics of biological growth.* New York: Springer, 2017.
24. Hao, Wenrui, and Avner Friedman. "The LDL-HDL profile determines the risk of atherosclerosis: a mathematical model." *PLoS ONE* 9 (2014).
25. Herrlin , Bo, and Sylvèn, Christopher. "Increased arterial oxygen content—an important compensatory mechanism in chronic moderate heart failure." *Cardiovascular research* 25 (1991): 384--390.
26. Holzapfel, GA, G Sommer, CT Gasser, and P. Regitnig. "Determination of layer-specific mechanical properties of human coronary arteries with nonatherosclerotic intimal thickening and related constitutive modeling." *American Journal of Physiology - Heart and Circulatory Physiology* 289, no. 5 (2005): H2048 - H2058.
27. Holzapfel, Gerhard A. *Nonlinear Solid Mechanics: A Continuum Approach for Engineering.* Chichester: John Wiley and Sons, 2000.
28. Huber, SA, P Sakkinen, D Conze, N Hardin, and R Tracy. "Interleukin-6 exacerbates early atherosclerosis in mice." *Arteriosclerosis, thrombosis, and vascular biology* 19, no. 10 (1999): 2364 - 2367.
29. Jackson, C. L., E. W. Raines, R. Ross, and M. A. Reidy. "Role of endogenous platelet-derived growth factor in arterial smooth muscle cell migration after balloon catheter injury." *Arteriosclerosis and thrombosis: a journal of vascular biology* 13, no. 8 (1993): 1218 - 1226.
30. Kubo, T., et al. "The Dynamic Nature of Coronary Artery Lesion Morphology Assessed by Serial Virtual Histology Intravascular Ultrasound Tissue

Characterization." *Journal of the American College of Cardiology* 55, no. 15 (2010): 1590 - 1597.
31. Langtangen, Hans Petter, and Anders Logg . *Solving PDEs in Python: The FEniCS Tutorial I.* Springer International Publishing, 2016.
32. Libby , Peter, Paul M Ridker, and Attilio Maseri. "Inflammation and atherosclerosis." *Circulation* 105 (2002): 1135--1143.
33. Loree, H. M., R. D. Kamm, R. G. Stringfellow, and R. T. Lee. "Effects of fibrous cap thickness on peak circumferential stress in model atherosclerotic vessels." *Circulation Research* 71, no. 4 (1992): 850 - 858.
34. Mair, Douglas D, and Donald G Ritter. "Factors influencing systemic arterial oxygen saturation in complete transposition of the great arteries." *American Journal of Cardiology* 31 (1973): 742--748.
35. Mallat, Zia, et al. "Protective role of interleukin-10 in atherosclerosis." *Circulation research* 85, no. 8 (1999): e17 - e24.
36. Mohammad Mirzaei, N., P.-W. Fok, and W. S. Weintraub. *An integrated approach to simulating the vulnerable atherosclerotic plaque.* arXiv:1910.00734, 2019.
37. Mohammad Mirzaei, Navid. "Finite element simulation of atherosclerotic plaque through morphoelasticity." 2020. https://cpb-us-w2.wpmucdn.com/sites.udel.edu/dist/e/8224/files/2020/07/thesis.pdf.
38. Mohammad Mirzaei, Navid, and Pak-Wing Fok. "Figshare." March 2020. https://doi.org/10.6084/m9.figshare.11968722.v3.
39. Nair, Anuja, Barry D. Kuban, Nancy Obuchowski, and D. Geoffrey Vince. "Assessing spectral algorithms to predict atherosclerotic plaque composition with normalized and raw intravascular ultrasound data." *Ultrasound in medicine and biology* (Springer) 10, no. 29 (2001): 1319-1331.
40. Pozzi, Silvia, and Christian Vergara. "Mathematical and numerical models of atherosclerotic plaque progression in carotid arteries." *ENUMATH2019 Proceedings. In press.*
41. Quarteroni , ALFIO, Andrea Manzoni, and Christian Vergara. "The cardiovascular system: mathematical modelling, numerical algorithms and clinical applications." *Acta Numerica* 26 (2017): 365--590.
42. Rubin, Stanley, Harvey V Brown, and HJ Swan. "Arterial oxygenation and arterial oxygen transport in chronic myocardial failure at rest, during exercise and after hydralazine treatment." *Circulation* 66 (1982): 143--148.
43. Simon, B.R., M.V. Kaufmann, M.A. McAfee, and A.L., Baldwin. "Finite element models for arterial wall mechanics." *Journal of biomechanical engineering* 115, no. 4B (1993): 489 - 496.
44. Stadius, Michael L., Reed Rowan, J. Franklin Fleischhauer, Robert Kernoff, Margaret Billingham, and Allen M. Gown. "Time course and cellular characteristics of the iliac artery response to acute balloon injury. An angiographic, morphometric, and immunocytochemical analysis in the cholesterol-fed New Zealand white rabbit." *Arteriosclerosis and thrombosis: a journal of vascular biology* 12, no. 11 (1992): 1267 - 1273.

45. Taylor, Charles A, and CA Figueroa. "Patient-specific modeling of cardiovascular mechanics." *Annual review of biomedical engineering* 11 (2009): 109--134.
46. Thon, MP, et al. "A multiphysics approach for modeling early atherosclerosis." *Biomechanics and modeling in mechanobiology* 17 (2018): 617--644.
47. Vandiver, R. "Effect of residual stress on peak cap stress in arteries." *Mathematical Biosciences and Engineering* 11, no. 5 (2014): 1199 - 1214.
48. Virmani, R., A.P. Burke, F.D. Kolodgie, and A. Farb. "Pathology of the Thin-Cap Fibroatheroma: a type of vulnerable plaque." *Journal of Interventional Cardiology* 16, no. 3 (2003): 267 - 272.
49. Virmani, R., A.P. Burke, F.D. Kolodgie, and A. Farb. "Vulnerable plaque: the pathology of unstable coronary lesions." *Journal of interventional cardiology* 15, no. 6 (2002): 439-446.
50. Virmani, Renu, Jagat Narula, Martin B Leon, and James T Willerson. *The vulnerable atherosclerotic plaque: strategies for diagnosis and management.* John Wiley & Sons, 2008.
51. Yang, Yifan, Willi Jäger, Maria Neuss-Radu, and Thomas Richter. "Mathematical modeling and simulation of the evolution of plaques in blood vessels." *Journal of mathematical biology* 72, no. 4 (2016): 973 - 96.

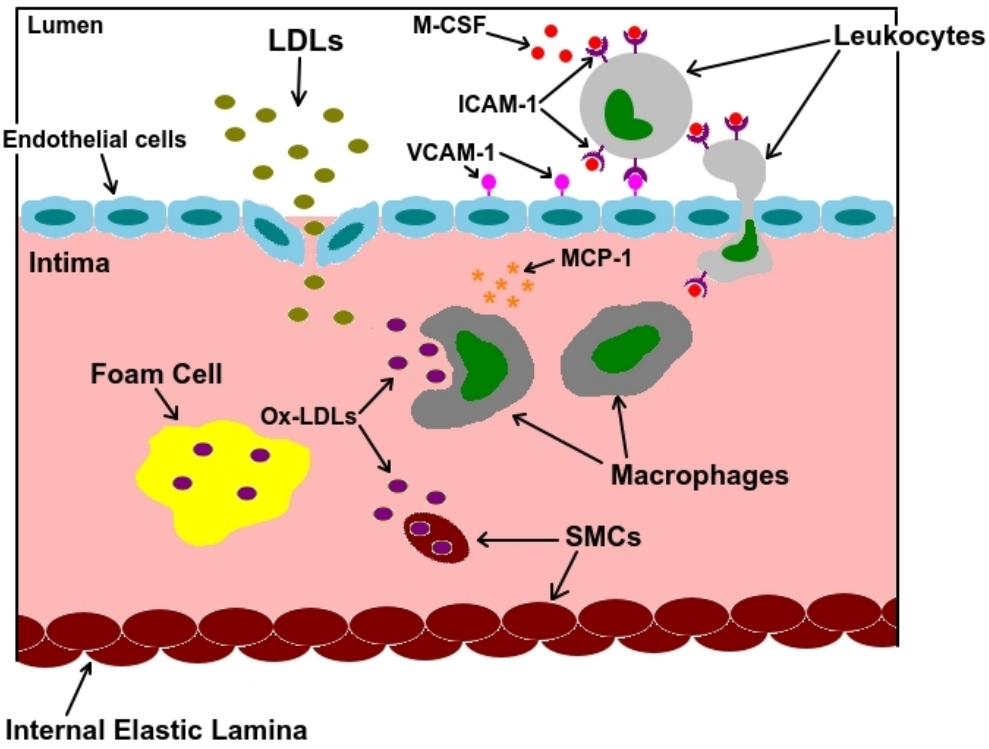

Figure 1: A summary of atherosclerosis microbiology. LDLs that enter the intima become Ox-LDLs and are consumed by macrophages leading to accumulation of foam cells. Foam cells later undergo necrosis and form a necrotic core.

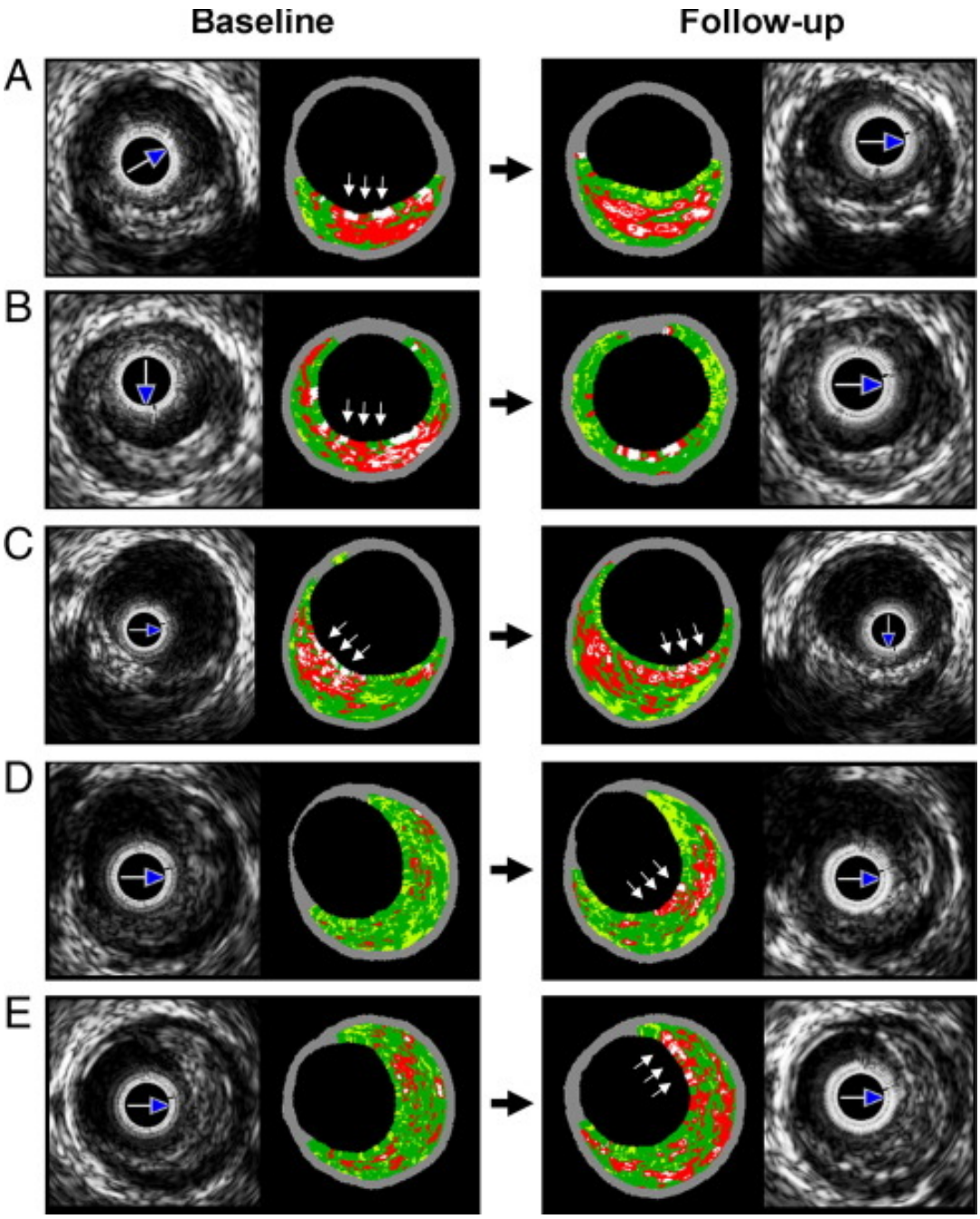

Figure 2: Serial images from (30). Baseline and follow-up were 12 months apart.

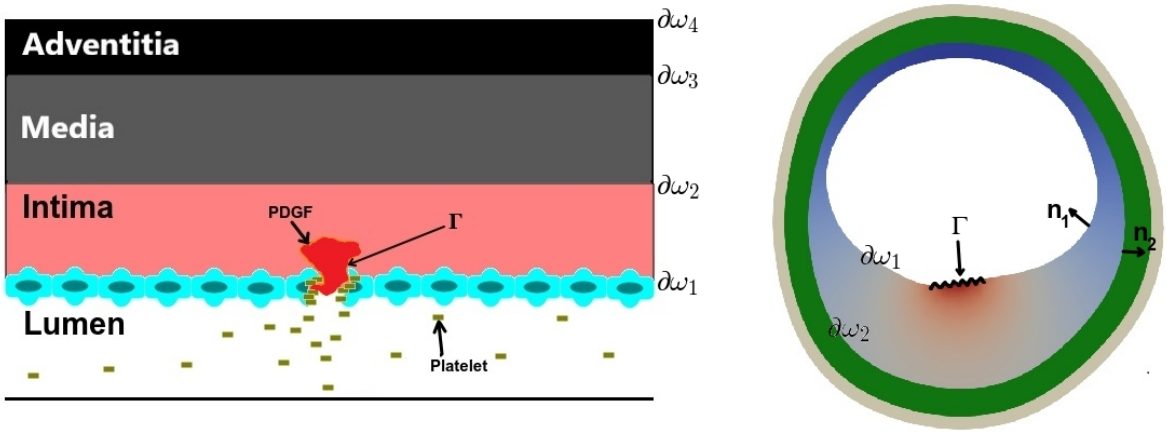

Figure 3: PDGF produced by platelets promote cell proliferation at the site of an injury.

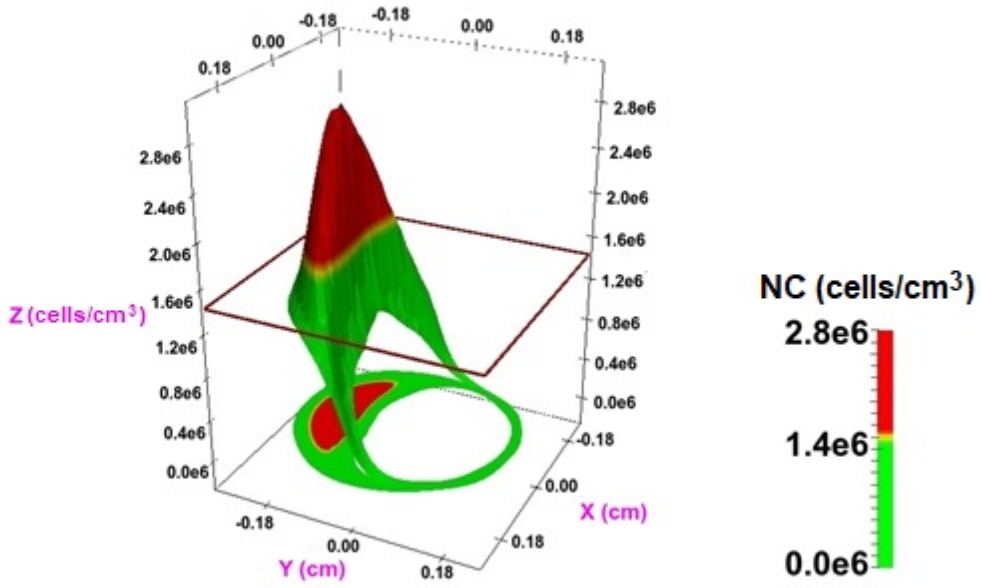

Figure 4: Solving the PDEs (1)-(5) produces smooth functions for biological quantities such as the necrotic cell density, N(x,y,t). By introducing a threshold value (here N = $1.4*10^6$), the function can be used to explain regions of necrosis in advanced fibroatheromas: N<$1.4*10^6$ indicates the presence of fibrotic tissue (green) while N>$1.4*10^6$indicates the presence of necrotic tissue (red). The 3D surface N(x,y,t) can be projected onto the xy plane to recreate the 2D IVUS cross sections in Figure 2.

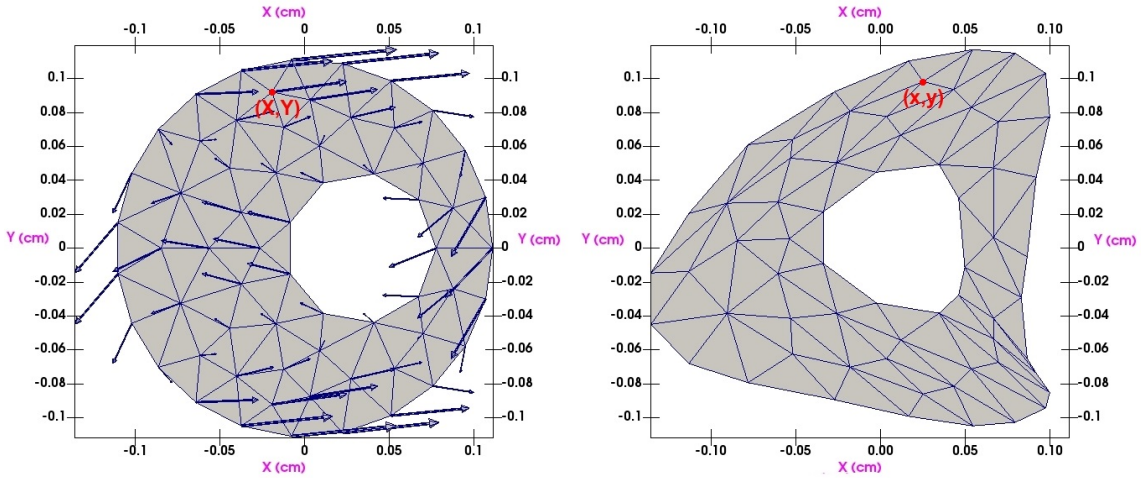

Figure 5: Minizing the energy (17) produces a displacement field (indicated by arrows) that deforms the arterial cross section.

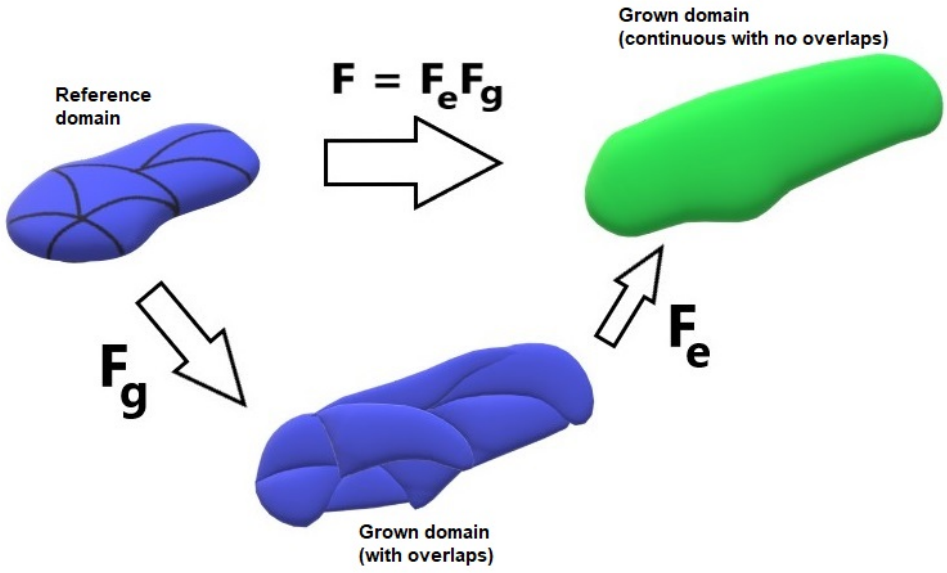

Figure 6: Decomposition of the deformation gradient F into a pure growth and an elastic response. This is the fundamental assumption in morphoelasticity theory: see Eq. (19).

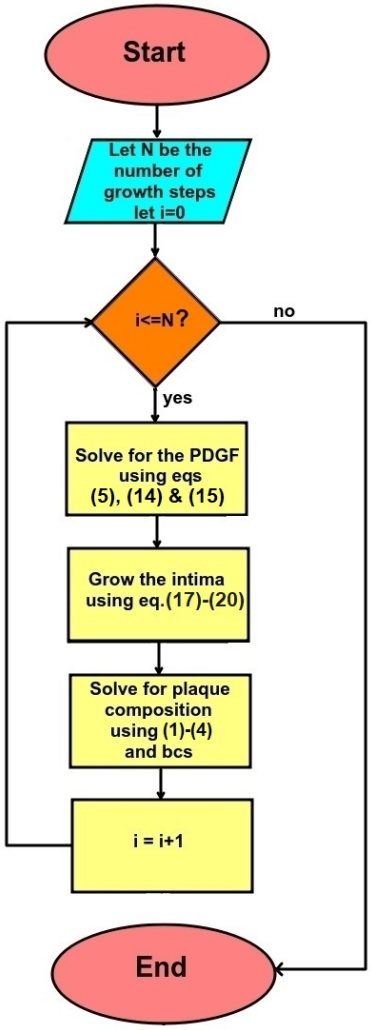

Figure 7: Flowchart of atherosclerosis simulation algorithm.

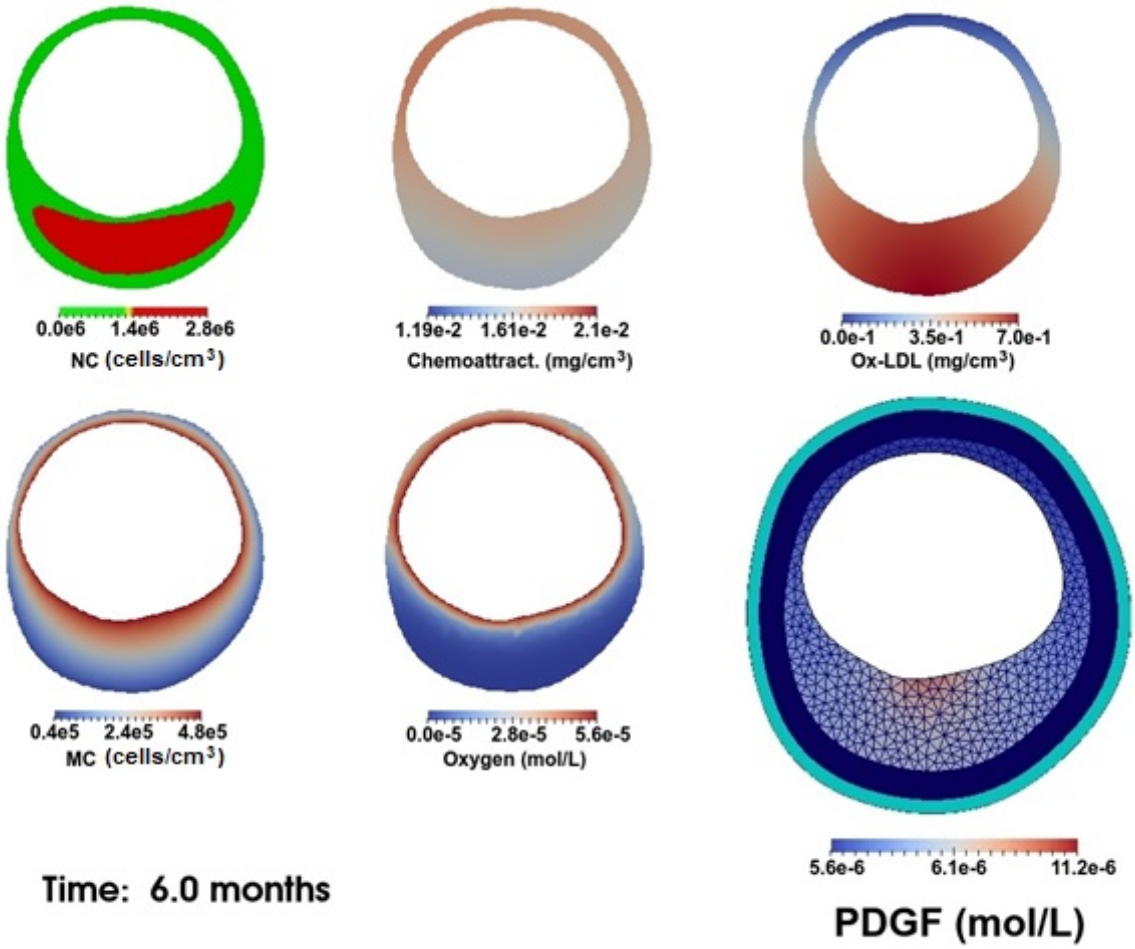

Figure 8: Typical plaque model results. Concentrations of NC, Chemoattractant, Ox-LDL, MC and and oxygen are outputted as spatially dependent fields distributed within the intima. For PDGF concentration, the media and adventitia are also indicated along with the finite element mesh.

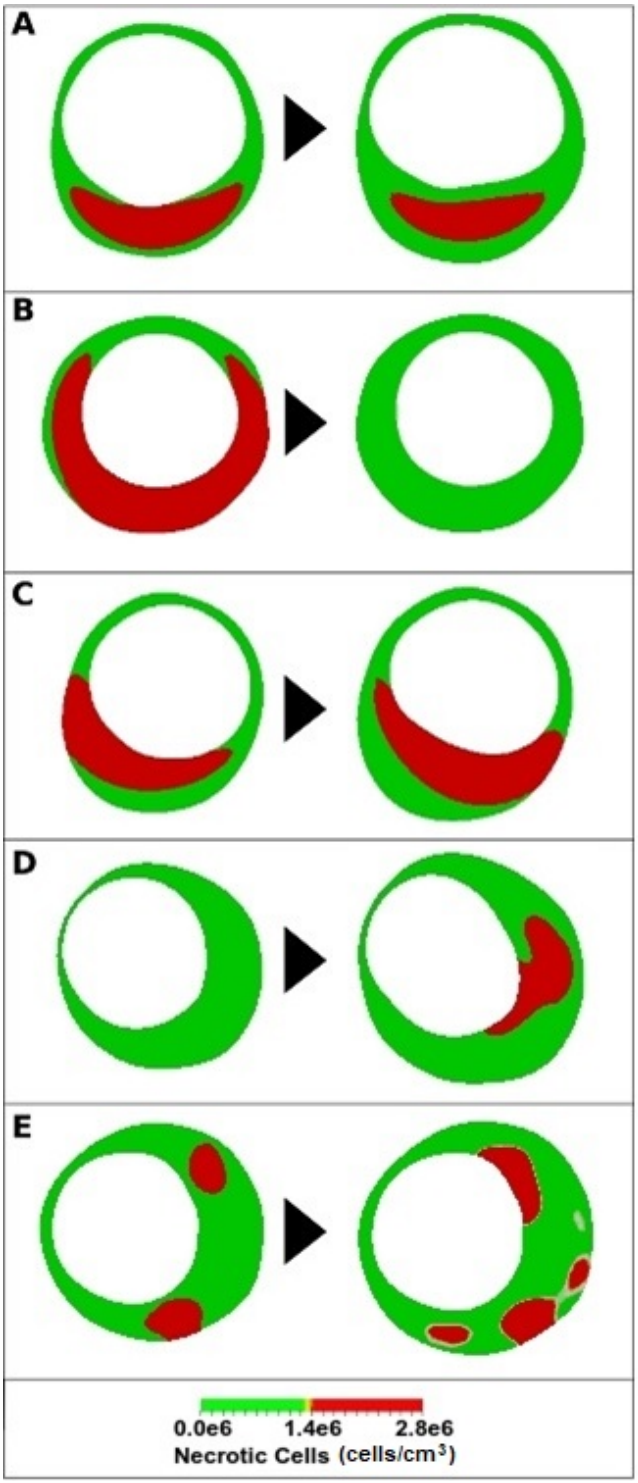

Figure 9: Simulations of necrotic core development in a coronary artery (compare with Fig. 2)

Symbol	Meaning	Case A	Case B	Case C	Case D	Case E	Units
μ	Chemotactic coefficient of MCs	2.26	7.77	4.41	9.17	6.02	$(mm^2/day).(cm^3/mg)$
D_1	Diffusivity of NCs	3.2×10^{-3}	3.3×10^{-3}	3.6×10^{-3}	3.9×10^{-3}	4.3×10^{-3}	cm^2/day
D_2	Diffusivity of MCs	1.72	1.74	1.92	2.06	2.30	cm^2/day
D_3	Diffusivity of CKs	80.8	81.6	89.7	96.3	107.6	cm^2/day
D_4	Diffusivity of O_2	172.5	174.3	191.6	205.8	229.9	cm^2/day
D_5	Diffusivity of PDGF	19.4	0	32.3	15.4	21.5	cm^2/day
β_1	Clearance rate of NCs	0.1	0.1	0.1	0.1	0.1	day^{-1}
β_2	Clearance rate of CKs	10	10	10	10	10	day^{-1}
β_3	Background O_2	1.2×10^4	1.2×10^4	1.2×10^4	1.2×10^4	1.2×10^4	day^{-1}

Table 1: Parameter values for Eqs (1)-(5) used to generate Figure 9. Abbreviations: MC = Macrophage Cells, NC = Necrotic Cells, CKs = Chemokines, O_2 = Oxygen, PDGF = Platelet Derived Growth Factor.

	consumption rate						
β_4	Decay rate of PDGF	2	0	2	2	2	day^{-1}
χ_1	Production rate of CKs	2.5×10^{-6}	2.5×10^{-6}	2.5×10^{-6}	2.5×10^{-6}	2.5×10^{-6}	cm^3/day
χ_2	Consumption rate of O_2 by MCs	2.5×10^{-7}	2.5×10^{-7}	2.5×10^{-7}	2.5×10^{-3}	2.5×10^{-7}	cm^3/day
γ_{min}	Normoxic MC death rate	3×10^{-3}	3×10^{-3}	3×10^{-3}	3×10^{-3}	3×10^{-3}	1/day
γ_{max}	Hypoxic MC death rate	1.2	1.2	1.2	1.2	1.2	1/day
P_0	PDGF BC	1.4×10^{-3}	0	10^{-3}	0.28×10^{-3}	0.45×10^{-3}	mg/cm^3
n	# Injury Points	1	0	1	2	1	none
p	Lumen Pressure	120	120	120	120	120	mmHg

Table 2: Time-dependent parameters for Mechanisms 1-4.

	Meaning	Case A	Case B	Case C	Case D	Case E	Units
$L(x,y,t)$	Ox-LDL concentration	Static	Decreasing in time	Location changes in time	Increasing in time	Static	mg/cm^3
$M_0(t)$	Macrophage density in endothelium	Increases from 4.6×10^5 to 4.64×10^5	Decreases from 5.2×10^5 to 1.2×10^5	4×10^5	Increases from 0 to 1.7×10^5	4.2×10^5	$cells/cm^3$
$C_0(t)$	O_2 density in endothelium	Increases from 5.6×10^{-5} to 11.2×10^{-5}	5.6×10^{-5}	5.6×10^{-5}	N/A	N/A	mol/L

$f(x,y,t)$	O_2 sources within intima	0	0	0	6.7	Sum of Gaussian functions[1]	mol/L/day

[1] Specifically, $f(x,y,t) = \sum_{k=1}^{N} f_k(t) \exp\left[-a_k(x-x_k)^2 - b_k(y-y_k)^2\right]$ for some constants a_k, b_k, N, x_k, y_k and time-dependent functions $f_k(t)$.